J Nanopart Res (2012) 14:964
DOI 10.1007/s11051-012-0964-8

RESEARCH PAPER

Synthesis optimization and characterization of chitosan-coated iron oxide nanoparticles produced for biomedical applications

Gozde Unsoy · Serap Yalcin · Rouhollah Khodadust · Gungor Gunduz · Ufuk Gunduz

Received: 21 January 2012 / Accepted: 30 May 2012 / Published online: 6 October 2012

Abstract The chitosan-coated magnetic nanoparticles (CS MNPs) were in situ synthesized by cross-linking method. In this method; during the adsorption of cationic chitosan molecules onto the surface of anionic magnetic nanoparticles (MNPs) with electrostatic interactions, tripolyphosphate (TPP) is added for ionic cross-linking of the chitosan molecules with each other. The characterization of synthesized nanoparticles was performed by X-ray diffraction (XRD), X-ray photoelectron spectroscopy (XPS/ESCA), Fourier transform infrared spectroscopy (FTIR), transmission electron microscopy (TEM), dynamic light scattering (DLS), thermal gravimetric analysis (TGA), and vibrating sample magnetometry (VSM) analyses. The XRD and XPS analyses proved that the synthesized iron oxide was magnetite (Fe_3O_4). The layer of chitosan on the magnetite surface was confirmed by FTIR. TEM results demonstrated a spherical morphology. In the synthesis, at higher NH_4OH concentrations, smaller sized nanoparticles were obtained. The average diameters were generally between 2 and 8 nm for CS MNPs in TEM and between 58 and 103 nm in DLS. The average diameters of bare MNPs were found as around 18 nm both in TEM and DLS. TGA results indicated that the chitosan content of CS MNPs were between 15 and 23 % by weight. Bare and CS MNPs were superparamagnetic. These nanoparticles were found non-cytotoxic on cancer cell lines (SiHa, HeLa). The synthesized MNPs have many potential applications in biomedicine including targeted drug delivery, magnetic resonance imaging (MRI), and magnetic hyperthermia.

Keywords Iron oxide (Fe_3O_4) · Chitosan · Magnetic nanoparticle · Biomedicine

Abbreviations

MNPs	Magnetic nanoparticles, magnetite, Fe_3O_4
CS MNPs	Chitosan-coated magnetic nanoparticles
CS	Chitosan
TPP	Tripolyphosphate
XRD	X-ray diffraction
XPS/ESCA	X-ray photoelectron spectroscopy
FTIR	Fourier transform infrared spectroscopy
TEM	Transmission electron microscopy
DLS	Dynamic light scattering

G. Unsoy (✉) · R. Khodadust
Department of Biotechnology, Middle East Technical University, Ankara 06800, Turkey
e-mail: gozdeunsoy@hotmail.com

S. Yalcin · U. Gunduz (✉)
Department of Biological Sciences, Middle East Technical University, Ankara 06800, Turkey
e-mail: ufukg@metu.edu.tr

S. Yalcin
Kaman Vocational High School, Ahi Evran University, Kırşehir 40000, Turkey

G. Gunduz
Department of Chemical Engineering, Middle East Technical University, Ankara 06800, Turkey

TGA	Thermal gravimetric analysis
VSM	Vibrating sample magnetometry
Ms	Saturated magnetization
MRI	Magnetic resonance imaging
SPIONs	Superparamagnetic iron oxide nanoparticles (50–180 nm)
USPIONs	Ultrasmall superparamagnetic iron oxide nanoparticles (10–50 nm)
VSPIONs	Very small superparamagnetic iron oxide nanoparticles (<10 nm)

Introduction

The synthesis and characterization of nanoparticles have been the focus of an intensive research for more than 10 years. Biochemically functionalized nanoparticles can be used in many different biomedical applications, such as targeted drug delivery, hyperthermia, and MR imaging (Allen and Cullis 2004; Prabaharan and Mano 2005). Nanoparticles, used in biomedical applications, must be biocompatible, nontoxic, and non-immunogenic. Their particle size must be small enough to remain in the circulation after the internalization to pass through the capillary systems of tissues avoiding vessel embolism for a successful application. It has been found that the size of the nanoparticles plays a key role in their adhesion to and interaction with the cells. The possible mechanisms for the particles to pass through the physiological barriers could be paracellular passage (<50 nm), endocytotic uptake (<500 nm), and lymphatic uptake (particle size <5 μm) (Florence et al. 1995; Lefevre et al. 1978; Sanders and Ashworth, 1961) Magnetic nanoparticles (MNP) have been extensively studied according to their specific properties (non-toxicity, nano sizes, etc.) in biomedical applications (Li et al. 2008; Denkbas et al. 2002). With respect to size, it is generally agreed that nanoparticles with a hydrodynamic diameter of 10–100 nm are pharmacokinetically optimal for in vivo applications. MNPs are preferred to be superparamagnetic and have high magnetization property so that their movement in the blood can be controlled with external magnetic field and be immobilized close to the targeted tissue (Gupta and Wells 2004).

Iron oxide nanoparticles (Fe_2O_3 and Fe_3O_4), being biodegradable and suitable for surface modifications, are the most prominent class of MNPs for biomedical applications such as in vivo magnetic resonance imaging (Weissleder et al. 1997), magnetic hyperthermia for cancer treatment, and tissue-specific delivery of therapeutic agents (Lubbe et al. 1996; Veiseh et al. 2010; Singh et al. 2011). Two other advantages of iron oxide nanoparticles are their low toxicity on cells and superparamagnetic properties. Superparamagnetic nanoparticles exhibit outstanding magnetic properties because they show no magnetization in the absence of a magnetic field but become strongly magnetized in the presence of magnetic field. Superparamagnetic nanoparticles can be organized according to their hydrodynamic diameter into several categories (Corot et al. 2006) standard superparamagnetic iron oxide nanoparticles (SPIONs) (50–180 nm), ultrasmall superparamagnetic iron oxide nanoparticles (USPIONs) (10–50 nm), and very small superparamagnetic iron oxide nanoparticles (VSPIONs) (<10 nm) (Weinstein et al. 2010).

The approaches to synthesize iron oxide nanoparticles can be top down (mechanical attrition) and bottom up (chemical synthesis). Chemical synthesis is better to produce uniformly sized and shaped nanoparticles. This can be subcategorized into two major chemical processes: coprecipitation and thermal decomposition. Coprecipitation method was preferred in this study for magnetic iron oxide nanoparticle synthesis because of its potential for large-scale manufacturing, cost-effectiveness, ease of production, and hydrophilicity of nanocrystals (Massart and Cabuil 1987). Hydrophilicity of nanoparticles is a key requirement for biomedical applications.

Surfactants are used to coat magnetic nanoparticles to prevent aggregation caused by magnetic dipole–dipole attractions between particles (Li et al. 2008; Denkbas et al. 2002). Functionality of MNPs is largely dependent on the properties of their surface coatings, which change the surface charge of nanoparticle, reduce the risk of immunogenicity, and increase the cellular uptake. Among the coating materials studied to date, chitosan has drawn considerable attention.

Chitosan, made from naturally occurring chitin, is a biodegradable, biocompatible, linear polysaccharide and has many reactive functional groups that can serve as an anchor for conjugation of therapeutics, targeting ligands, and imaging agents. In comparison with many other polymers, the chitosan backbone contains a

number of free amine groups, which allow binding of many agents.

For biomedical applications, chitosan-coated magnetic nanoparticles (CS MNPs) are generally synthesized by in situ coating method which is alkaline coprecipitation of Fe(II) and Fe(III) precursors in aqueous solutions of hydrophilic chitosan polymers. These polymers serve to limit the core growth of iron oxide during the preparation, to stabilize via steric repulsions when the nanoparticles disperse in aqueous media, and to reduce the opsonization process in vivo (Mornet et al. 2004).

In this study, in situ synthesis method was used for the preparation of CS MNPs, involving the coprecipitation of iron salts in the presence of chitosan and tripolyphosphate. In an acidic environment, the amino groups could be positively charged after protonation. Therefore, chitosan is able to interact with negatively charged molecules (Calvo et al. 1997), such as the hydroxyl (Fe–OH) groups on the surface of magnetite nanoparticles. Sodium tripolyphosphate (TPP) is a polyvalent anion with three negatively charged phosphate groups. The hydrophilic Fe_3O_4 cores precipitate by forming nuclei with high surface energies and rapidly adsorb well-dissolved chitosan polymers. The addition of TPP cross-links the adsorbed chitosan molecules to each other through the ionic interactions between the positively charged amino groups of chitosan and negatively charged TPP. Under these conditions, uniform layers of chitosan polymers were assembled by physical cross-linking induced by electrostatic interaction on Fe_3O_4 cores to stabilize each discrete nanoparticle. The CS MNPs synthesized through this method are monodispersed and their surface is uniformly coated with low molecular weight chitosan polymer.

Experimental

Materials

Iron (II) chloride tetrahydride ($FeCl_2{\cdot}4H_2O$), iron (III) chloride hexahydrate ($FeCl_3{\cdot}6H_2O$), acetic acid (CH_3COOH), and ammonium hydroxide (NH_4OH) were obtained from Merck, Germany; chitosan (LMW, 85 % deacetylated) and sodium tripolyphosphate (TPP) were purchased from Sigma-Aldrich Chemie GmbH, Germany.

Synthesis of magnetic iron oxide nanoparticles

Magnetic iron oxide (Fe_3O_4) nanoparticles were synthesized for comparison purpose by the coprecipitation of Fe(II) and Fe(III) salts at 1:2 ratio in 150 ml deionized water within a five-necked glass balloon. Glass balloon is placed on a heating mantle and stirred by a glass rod of mechanical stirrer, which is inserted into the middle neck of the balloon. It is vigorously stirred in the presence of nitrogen (N_2) gas at 90 °C. The nitrogen gas prevents oxidation. Ammonium hydroxide (NH_4OH) is added to the system dropwise. The process ends by washing with deionized H_2O until the solution pH is 9.0.

In situ synthesis of chitosan-coated magnetic iron oxide nanoparticles

Chitosan-coated magnetic iron oxide nanoparticles (Fig. 1) were in situ synthesized by the coprecipitation of Fe(II) and Fe(III) salts in the presence of chitosan and TPP molecules with some modifications of Kavaz et al. (2010). TPP was used for the cross-linking of low molecular weight chitosan polymers.

Chitosan (0.15 g) was dissolved in 30 ml of 1 % acetic acid, and the pH was adjusted to 4.8 by 10 M NaOH. Iron salts (1.34 g of $FeCl_2{\cdot}4H_2O$ and 3.40 g of $FeCl_3{\cdot}6H_2O$) were dissolved in 30 ml of 0.5 % chitosan solution. Under the nitrogen (N_2) gas flow and by vigorously stirring at 2500 rpm, 10 ml of 7.5 % TPP and different amounts of 32 % NH_4OH (18, 20, 25, and 30 ml) were added to the solution to obtain the final NH_4OH concentrations of 31 % (CS MNP-S_1), 33 % (CS MNP-S_2), 38.5 % (CS MNP-S_3), and 43 % (CS MNP-S_4) at room temperature. The ammonia solution was added very slowly to produce smaller sized nanoparticles. The resulting solution was stirred for an additional 1 h. The colloidal chitosan-coated magnetic Fe_3O_4 nanoparticles were extensively washed with deionized water and separated by magnetic decantation for several times.

Characterization of synthesized bare and chitosan-coated magnetic Fe_3O_4 nanoparticles

Crystal structures of synthesized MNPs were analyzed by XRD. The chemical groups and chemical interactions involved in synthesized MNPs were identified

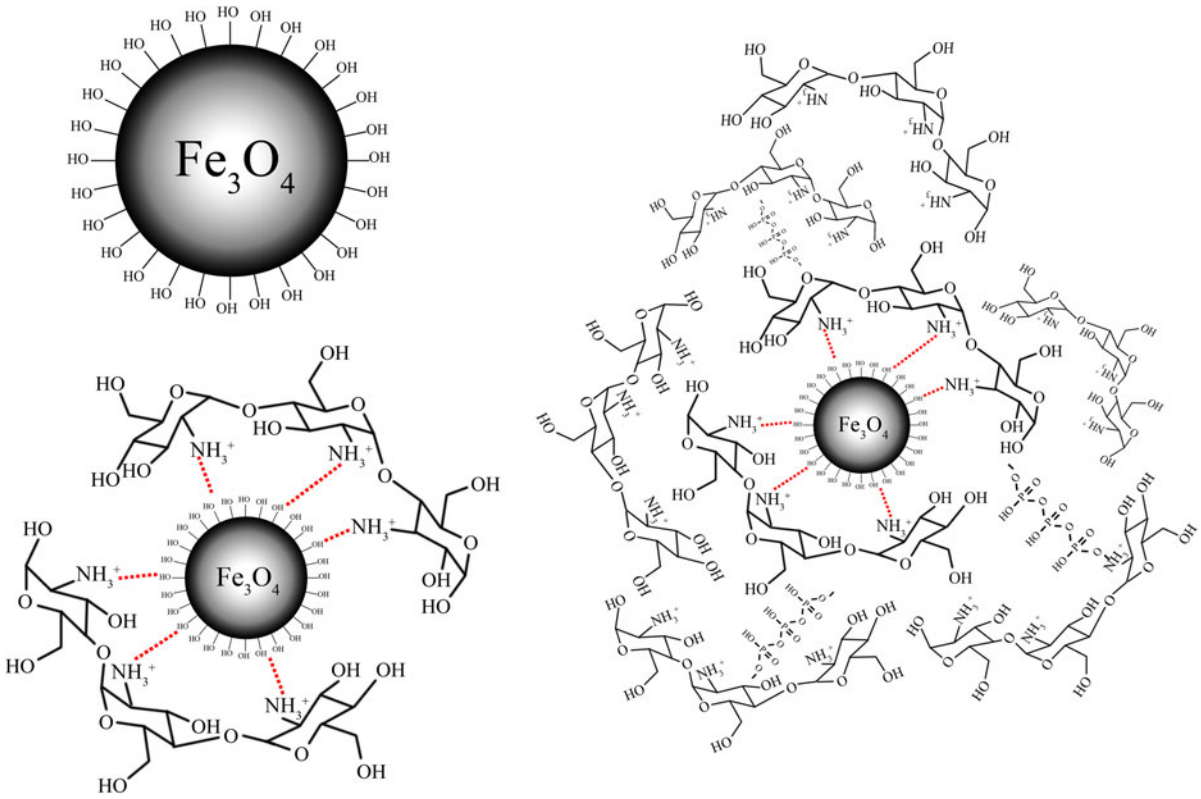

Fig. 1 Schema of in situ synthesized chitosan-coated magnetic nanoparticles (CS MNPs)

using the FTIR and XPS methods. The sizes of magnetic core and morphological properties were observed through TEM images. The hydrodynamic sizes were determined with DLS measurements. The qualitative and quantitative information about the volatile compounds of the nanoparticles has been provided by TGA–FTIR. Magnetic properties of MNPs were determined through VSM analyses.

Results

In the synthesis of bare MNPs, the conditions have been optimized by adjusting the temperature (20–90 °C by 10 °C intervals). Crystal structures were formed at the temperatures >50 °C. Pure Fe_3O_4 was obtained at 90 °C. In the synthesis of CS MNPs, the effect of NH_4OH amount (18, 20, 25, and 30 ml) was studied. Different sized CS MNPs were obtained (2–8 nm) by changing the conditions. The characteristic properties of synthesized bare and CS MNPs have been analyzed by various analytical methods.

X-ray diffraction (XRD)

The crystal structure of synthesized iron oxide (Fe_3O_4) nanoparticles was determined by XRD. The diffractogram was given in Fig. 2. Diffraction peaks at (220), (311), (400), (422), (511), (440), and (533), which are the characteristic peaks of the magnetite (Fe_3O_4) crystal having an inverse cubic spinel structure by comparison with standards (JCPDS card, file No. 77-1545), appeared in both bare and chitosan-coated nanoparticles (Das et al. 2008). The XRD spectrum of chitosan is given at several reports in the literature (Li et al. 2005; Lu et al. 2007) which shows peaks with low intensity/cps values around $2\theta = 10^{\circ}$ and a broad peak at around $2\theta = 15^{\circ}$–35°. In Fig. 2, the characteristic peak corresponding to chitosan is marked with "x".

XRD results revealed the presence of the Fe_3O_4 crystals in both types of the synthesized magnetite nanoparticles. The peak positions were unchanged, which illustrated that the chitosan binding process did not result in the phase change of Fe_3O_4.

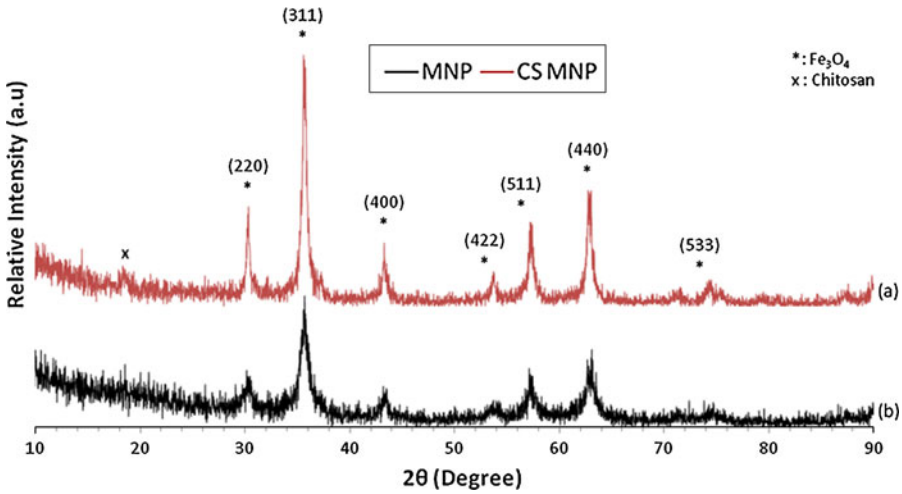

Fig. 2 XRD patterns of (**a**) chitosan-coated MNP–S_1 (31 %) and (**b**) bare MNP

The particle sizes can be quantitatively evaluated from the XRD data using the Debye–Scherrer equation, which gives a relationship between peak broadening in XRD and particle size. $D = k\lambda/(\beta\cdot\cos\theta)$, where k is Sherrer constant (0.89), λ is the X-ray wavelength (nm), β is the peak width of half-maximum, and θ is the Bragg diffraction angle. The crystallite sizes of the Fe_3O_4 and chitosan-coated Fe_3O_4 nanospheres obtained from this equation were found to be about 18 and 8 nm, respectively.

X-ray photoelectron (XPS)

Because both Fe_3O_4 (magnetite) and γ-Fe_2O_3 (maghemite) possess the inverse spinel structure, they can have similar XRD patterns. So, XRD by itself is not an ideal method to discriminate the certain crystalline forms of iron-containing nanoparticles, such as Fe_3O_4 and γ-Fe_2O_3. XPS was then used to examine shell structure of the synthesized product because core electron lines of ferrous and ferric ions can both be detectable and distinguishable in XPS. Figure 3 shows representative XPS spectra of the synthesized products. The photoelectron peaks at 711.7 and 725.2 eV are the characteristic doublet of Fe $2p^{3/2}$ and $2p^{1/2}$ core-level spectra of iron oxide, respectively, which is consistent with the oxidation state of Fe in Fe_3O_4. These peaks at 711.7 and 725.2 eV were observed in both bare MNPs (Fig. 3a) and chitosan-coated MNPs (Fig. 3b) (Teng et al. 2003; Liu et al. 2010; Daou et al. 2006).

XPS spectra can identify the absorption sites and the interactions between MNP and CS by the bands obtained from their spectrum. There is no significant peak observed for amino groups in bare MNPs (Fig. 3a). The XPS spectrum of CS MNP complex was shown in Fig. 3b. The N1s band of chitosan at 397.7 eV is assigned to amino groups ($–NH_2$). In CS MNPs, the binding energy at 398 eV was attributed to the amino groups that were involved in hydrogen bond (NH_2–O) which reflects the presence of amino groups of chitosan. The CS MNP complex expressed a new band for N1s at around 400 eV. This new band was assigned to chelation between the amino groups and iron ions (NH_2–Fe). The chelation of CS–Fe_3O_4 demonstrates that the magnetite was coated with chitosan (Wang et al. 2009).

Fourier transform infrared spectroscopy (FTIR)

To confirm the chemical composition of synthesized nanoparticles, FTIR spectra were obtained. The FTIR results were given with their auto baseline corrections. The presence of Fe_3O_4 core could be identified by the strong stretching absorption band at 579 cm^{-1}, which corresponded to the Fe–O bond (Fig. 4c). The peak located in the 583 cm^{-1} region is found in bare and chitosan-coated nanoparticle's spectra, confirming that the products contain magnetite. The peaks around 1615 ± 15 cm^{-1}, assigned to the NH_2 group bend scissoring, are present in both chitosan and chitosan-coated nanoparticle's spectra, proving that magnetite nanoparticles were successfully coated by chitosan polymer (Coates 2000). In the IR spectrum of chitosan (Fig. 4a), the band at 1628 cm^{-1} is assigned to NH_2 group bend scissoring, the peak at 1422 cm^{-1} to OH

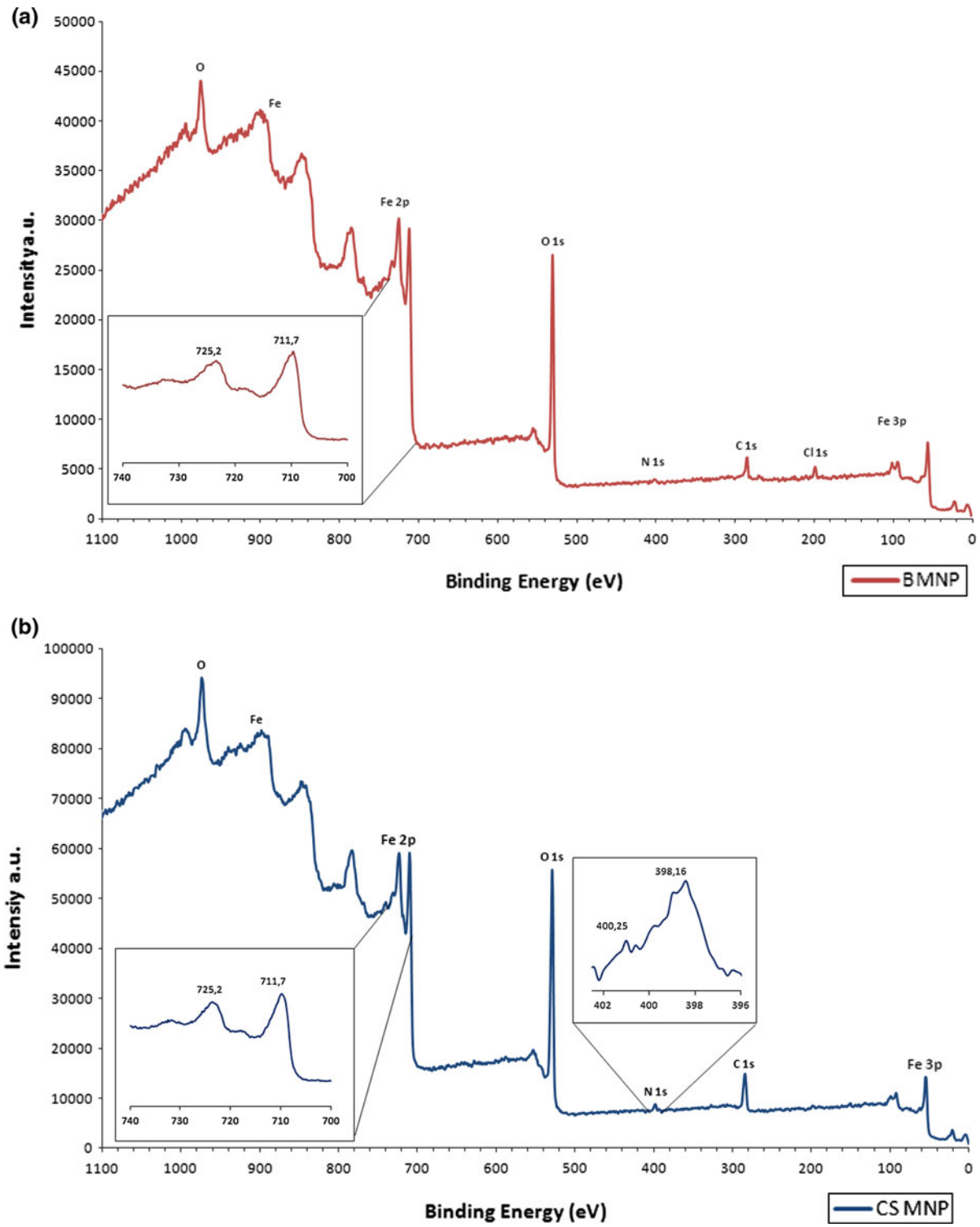

Fig. 3 X-ray photoelectron spectra of the synthesized magnetic nanoparticles. (**a**) Bare MNP and (**b**) chitosan-coated MNP-S_1 (31 %). The *upper inset* is the expanded spectrum of N1s in CS MNPs. The *lower insets* are the expanded spectra of Fe 2p

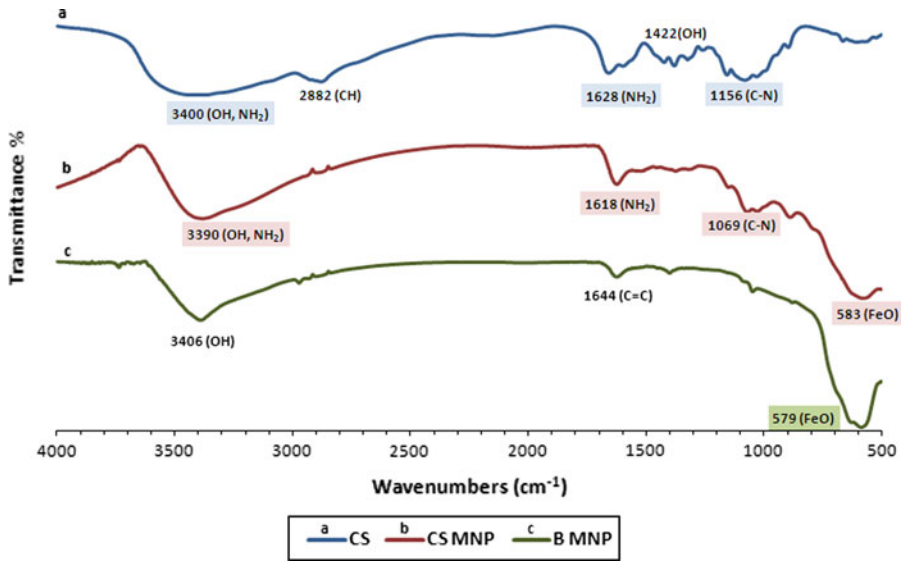

Fig. 4 Fourier transform infrared spectra of the chitosan and synthesized magnetic nanoparticles. (**a**) Chitosan. (**b**) Chitosan-coated MNP-S_1 (31 %). (**c**) Bare MNP

bending of primary alcoholic group, and 1156 cm^{-1} to C–N stretch in chitosan. In the spectrum of CS MNP (Fig. 4b), the 1628 cm^{-1} peak of NH_2 group bend scissoring in chitosan, shifted to 1618 cm^{-1} and a new sharp peak at 583 cm^{-1} was appeared. All characteristic peaks of chitosan and iron oxide were present in the spectrum of CS MNP. Results indicated that MNPs were successfully coated with chitosan and these results are compatible with the articles in the literature (Li et al. 2008; Zhang et al. 2010a; Ma et al. 2007).

Transmission electron microscopy (TEM)

Size and morphology of synthesized MNPs and CS MNPs have been observed by TEM. Obtained images showed that (Fig. 5a–c) the synthesized CS MNPs are almost spherical and have more uniform size distribution as compared with bare MNPs. The average diameters are around 18–20 nm (bare MNP), 6–8 nm (CS MNP-S_1), 5–7 nm (CS MNP-S_2), 3–5 nm (CS MNP-S_3), and 1–3 nm (CS MNP-S_4). The cumulative particle size distribution histograms of CS MNP-S_1 and CS MNP-S_3 were also given (Fig. 5d, e). The sizes of the nanoparticles get smaller as the concentration of NH_4OH increases in the solution during the synthesis. The monodispersity of size distribution and production of the smallest sized CS MNPs in the literature synthesized by this method are important features of this study. The ammonium concentration seems to be critical to obtain smaller sized nanoparticles.

Although it is difficult to directly observe the layer of CS on the MNPs from TEM images, the dispersing behavior of surface-stabilized MNPs (Fig. 5b, c) has been improved in comparison with that of bare MNPs (Fig. 5a), which exhibits aggregated morphology. Chitosan is a good agent for stabilizing aqueous suspension of bare MNPs because of its polyelectrolyte property.

The transmission electron microscopy revealed the parallel lattice fringes clearly visible at almost all the nanoparticles. The lattice spacing seen in the lattice fringe of the nanoparticles indicates the crystallinity and structural uniformity of the sample (Ye et al. 2006). The crystalline structures of the bare MNPs and CS MNPs were also characterized by powder X-ray diffraction (XRD) technique.

Dynamic light scattering (DLS)

DLS is concerned with measurement of particles suspended within a liquid. The average sizes of chitosan-coated MNPs were found as 103 nm CS MNP-S_1, 86 nm CS MNP-S_2, 66 nm CS MNP-S_3, and 58 nm CS MNP-S_4 in DLS measurements. These results are in parallel with the results obtained by TEM analyses. The average diameters of bare MNPs were

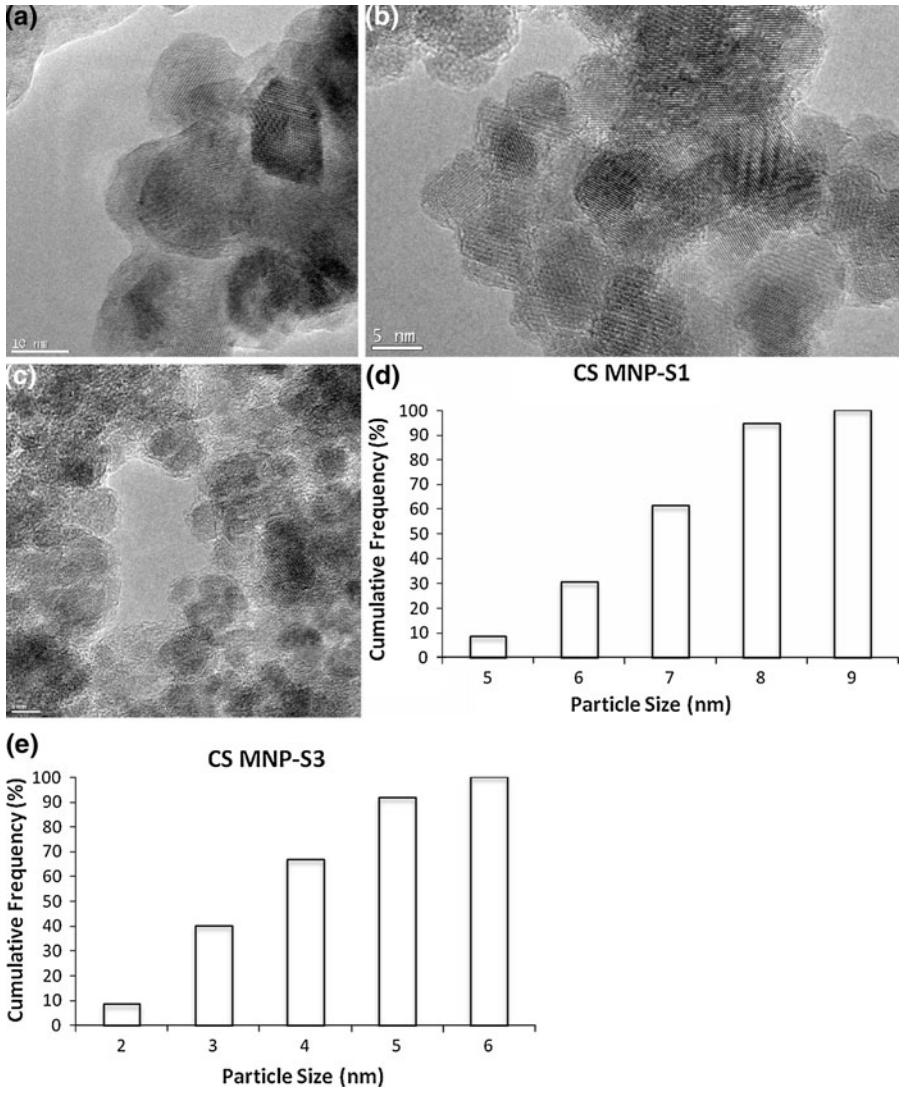

Fig. 5 TEM micrographs of (**a**) bare magnetite (Fe_3O_4), (**b**) CS MNP-S_1, (**c**) CS MNP-S_3 nanoparticles and cumulative particle size distribution (PSD) histograms of (**d**) CS MNP-S_1, (**e**) CS MNP-S_3

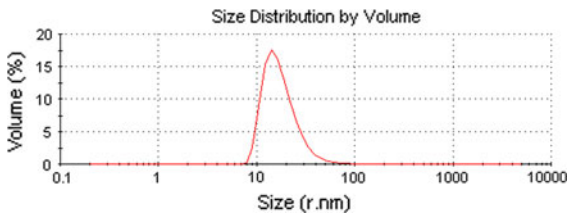

Fig. 6 Particle size distribution of bare MNPs

found as 18 nm, in both XRD and TEM results, their average sizes were also confirmed by DLS measurements (Fig. 6) since there was no polymer coating on the surface of MNPs, which will increase the hydrodynamic diameter of the nanoparticle.

Thermal gravimetric analysis (TGA and TGA–FTIR)

The TGA–FTIR analysis of bare and chitosan-coated Fe_3O_4 nanoparticles provides qualitative and quantitative information about the volatile components of the nanoparticles. The TGA curve (Fig. 7) shows that the weight loss of bare MNPs over the temperature range from 30 to 850 °C is about 3 %. This might be because of the loss of residual water in the sample.

The CS MNPs gave their distinctive TGA curves, which can provide indications of the content of chitosan polymers. The principle chains of CS began to degrade at about 250 °C and the final temperature of decomposition was around 700 °C. The results of

TGA–FTIR demonstrated that most of the organic layer, chitosan, was removed as CO_2 at high temperatures. The peaks at 2400–2000 cm^{-1} reflect O=C=O stretching assigned to carbonyl groups of CO_2 (Paama et al. 2003). From the percentage weight loss in the TGA curve, the amount of chitosan bound on MNPs was estimated. The average mass content of chitosan in nanoparticles by TGA was found to be about 23 % (CS MNP-S_1), 20 % (CS MNP-S_2), 17 % (CS MNP-S_3), and 15 % (CS MNP-S_4) (Fig. 7). With the decrease of NH_4OH percentage in the synthesis, the average diameters of magnetic CS MNPs increased from 58 to 103 nm and the chitosan content increased from 15 to 23 %.

Vibrating sample magnetometer (VSM)

Magnetic hysteresis curve is obtained by vibrating sample magnetometer. The applied magnetic field was changed and magnetization properties of synthesized Fe_3O_4 and chitosan-coated Fe_3O_4 nanoparticles were measured at 37 °C.

Figure 8 shows hysteresis loops of bare MNPs and CS MNP-S_1. The saturated magnetization (Ms) of bare magnetic nanoparticles is 62 emu/g, while the CS MNP-S_1 is about 39 emu/g (Fig. 8a). The decrease of Ms was because of the chitosan coating around MNPs. The existence of CS on the surface of MNP decreased the Ms because of the quenching of surface moments (Xu et al. 2007).

As it is seen from Fig. 8b, there is no remanence and coercivity observed in the hysteresis curves. This phenomenon proved that the MNPs showed superparamagnetic properties. The Ms values were obtained for CS MNP-S_1 (39 emu/g), CS MNP-S_2 (33 emu/g), CS MNP-S_3 (29 emu/g), and CS MNP-S_4 (25 emu/g). Because the weights of the CS MNPs used for the measurement of magnetic properties were constant, the decrease of Ms was because of the decreased core size of magnetite incorporated in the chitosan coating. The saturation magnetization of nanoparticles consistently increases with the size of the magnetic core (Maaz et al. 2007).

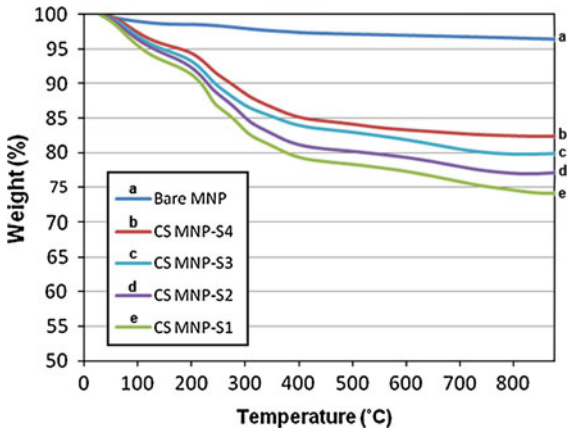

Fig. 7 Thermal gravimetric analysis curve of bare and chitosan-coated Fe_3O_4 nanoparticles

Cell proliferation assay with XTT reagent

To asses the cytotoxicities of synthesized bare MNPs and CS MNPs, cell proliferation assays were performed with XTT reagent on cervical carcinoma cell lines, HeLa and SiHa. The cell proliferation assay revealed that the synthesized bare and CS MNPs were not significantly cytotoxic on these cell lines. When the highest doses of bare MNPs and CS MNPs (1000 μg/ml) were applied on HeLa cells, cell proliferation decreased only 5 and 2 %, respectively (Fig. 9). Because the SiHa cells were more sensitive than HeLa cells, their cell proliferation rate decreased 8 %, at the highest dose (1000 μg/ml) of bare MNPs. The CS MNPs were also compatible with SiHa cells (Fig. 9), they decreased cell proliferation rates only 6 %.

Discussion

The synthesis of nanoparticles with small size and uniform size distribution is a subject of intensive research in recent years. In this study, CS MNPs were synthesized at four different ammonium ion concentrations. For each synthesis homogen size distributions were obtained at different size ranges. Smaller sized nanoparticles were obtained at higher ammonium concentrations. With the decrease of NH_4OH percentage in the synthesis, the average diameters of magnetic CS MNPs increased from 58 to 103 nm and the chitosan content by weight increased from 15 to 23 %.

Chitosan polymer is coated on iron oxide core by ionic cross-linking of TPP cross-linker with chitosan via electrostatic interactions. The coating of MNPs with a layer of chitosan was validated by FTIR. The ionic interactions occur between the negatively

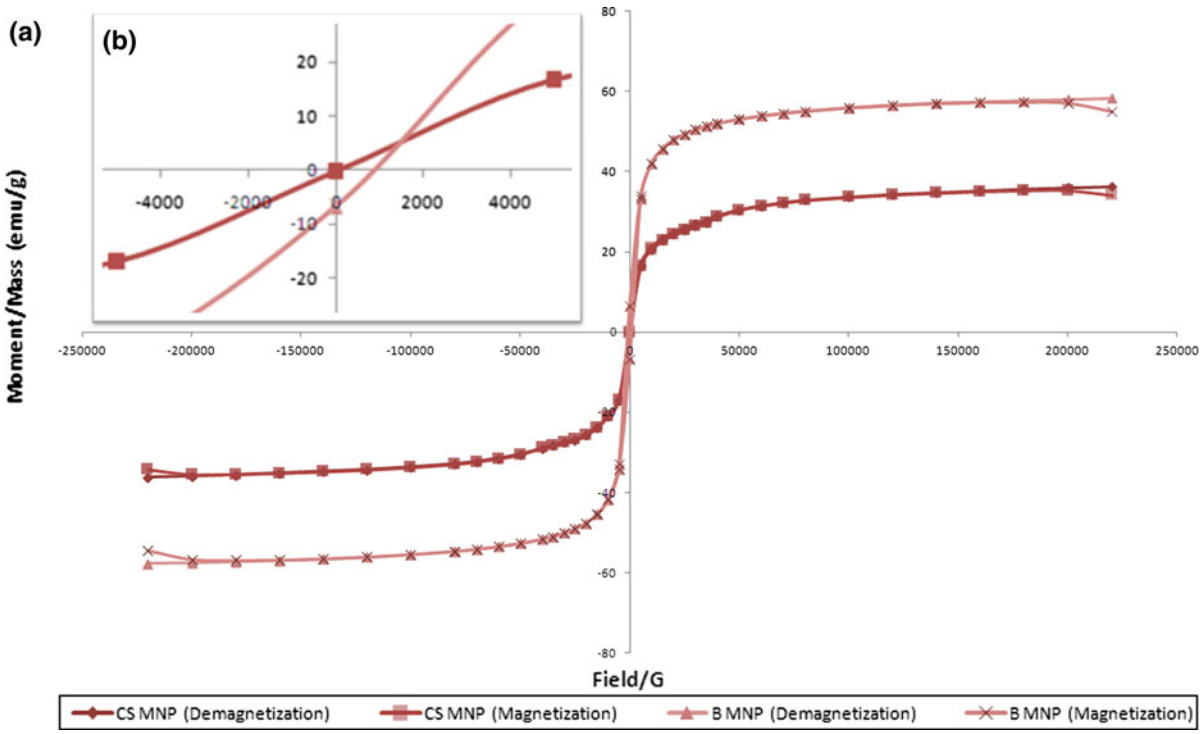

Fig. 8 Magnetic hysteresis loops of bare MNPs and CS MNP-S_1 (*a*). Zoom into the center of the hysteresis loops (*b*)

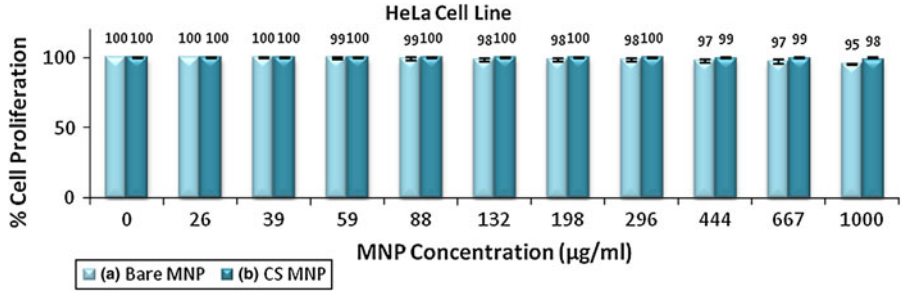

Fig. 9 Cell proliferation analyses (XTT) results of bare (*a*) and CS MNP-S_1 (*b*) on HeLa cells

charged (PO^-) groups of the cross-linker and the positively charged (NH_3^+) groups of chitosan molecules dissolved in aqueous acetic acid. This process leads to the formation of a densely packed structure yielding smaller sized nanoparticles as explained by Hritcu et al. (2009). Besides, $-NH_3^+$ groups of chitosan are attracted by $-OH^-$ of iron oxide, through this way nuclear growth of iron oxide is inhibited by chitosan molecules which provides smaller core size. Another important factor is the degree of deacetylation of chitosan. The higher deacetylation degree of chitosan can provide an increased number of free protonable amino groups (Hu et al. 2010). The CS MNPs have many reactive functional groups to load different molecules such as drugs, contrast agents, or targeting ligands for biomedical applications.

The resulting core magnetic nanoparticles were found as magnetite (Fe_3O_4) and had cubic spinal structures (Fig. 2). No evidence of impurities was found in the XRD pattern. The peaks shown in the XRD pattern of the prepared sample are sharp and intense, indicating good crystallinity of Fe_3O_4. These results are compatible with the XRD results in the literature (Dung et al. 2009). The XRD spectrum of chitosan is given at several reports in the literature (Li et al. 2005; Lu et al. 2007). Li et al. (2005) reported that chitosan raw material is essentially non-crystalline. In the case of cross-linked chitosan, the intensity

of characteristic peaks is even lower than that of pure chitosan, which was reported by Wan et al. (2003) and Lu et al. (2007). Because the chitosan is cross-linked by TPP in this study, the intensity of chitosan peak is very low in CS MNPs as it is seen in Fig. 2, as compatible with the literature. The differences in the diffraction patterns of chitosan and cross-linked chitosan could be attributed to modification in the arrangement of molecules in crystal lattice (Bhumkar and Pokharkar 2006). Chitosan nanoparticles were composed of a dense network structure of interpenetrating polymer chains cross-linked to each other by TPP.

The core sizes of synthesized CS MNPs, dependent on the preparation conditions, were found as 6–8 nm (CS MNP-S_1), 5–7 nm (CS MNP-S_2), 3–5 nm (CS MNP-S_3), and 1–3 nm (CS MNP-S_4) in TEM analyses. The estimated core size obtained from Debye–Scherrer equation was confirmed the particle sizes observed in TEM images. The total average sizes were found larger in DLS measurements. DLS method differs from TEM in that it measured the hydrodynamic particle size in the dispersion medium. TEM images show the core particle size, without the contribution of the chitosan; because the chitosan layer normally collapses onto the MNPs surface when the dispersion medium is evaporated prior to imaging. It is also obvious that the thickness of the stabilizing layer, when collapsed on the surface of the MNPs, is negligible. Therefore, the difference in diameter measurements obtained by DLS and those obtained by TEM is the size of the chitosan layer. However, this is only valid for small particles (diameter <200 nm) (Bhattarai et al. 2008).

Size-tunable synthesis of chitosan-coated magnetic nanoparticles by in situ coprecipitation method at this small size range is not reported in the literature. This method is advantageous than the earlier published methods (Tiaboonchai and Limpeanchob 2007) because the process is simple and carried out under mild conditions without using hazardous organic solvents. The nanoparticles obtained by our method are expected to have better biocompatibility than covalently cross-linked chitosan (Agnihotri et al. 2004; Park et al. 2010) as the chitosan was cross-linked with ionic interactions.

The magnetic Fe_3O_4–chitosan nanoparticles were in situ synthesized for lipase immobilization by Wu et al. (2009); however, their methods for synthesis were considerably different. Yuwei and Jianlong (2011) synthesized magnetic chitosan nanoparticles by in situ coprecipitation method without TPP for cupper removal. In their study, the particle size was found to have much wider size distribution.

Magnetic nanoparticles having a core size <30 nm show superparamagnetic behavior having remanence and coercivity nearly zero. In this study, magnetization characteristics of the nanoparticles were demonstrated by VSM analyses. No significant remanence and coercivity were observed in the hysteresis loops of bare and chitosan-coated MNPs. This phenomenon proved that MNPs synthesized in this study are superparamagnetic. In the absence of a magnetic field, superparamagnetic nanoparticles will not show magnetic properties. This is a desired characteristics in biomedical applications.

These superparamagnetic magnetite (Fe_3O_4) nanoparticles, stabilized by the biocompatible CS dispersant, have many potential applications in biomedicine. Being easily targetable in the magnetic field and having high surface to volume ratio, synthesized small nanoparticles can be efficiently used for imaging, diagnosis, and therapy purposes (Yezhelyev et al. 2006; Pison et al. 2006).

In the literature, similarly synthesized nanoparticles generally show some agglomeration (Li et al. 2008; Dung et al. 2009; Zhang et al. 2010b). However, in this study, because of the smaller particle sizes, nanoparticles have very large surface area and this surface energy could increase the agglomeration. Therefore, during the synthesis of CS MNPs, larger nanoparticles were obtained by increasing concentration of ammonia solution. The increase in the particle sizes of CS MNP-S_1 resulted in less agglomeration, which is observed in TEM images. Dissolving CS MNPs at various solvents such as PBS or ultrasonication after synthesis could help to overcome the agglomeration problem. The agglomeration can be reduced after loading with various therapeutics, because of the changes in size and charge of nanoparticles. The studies to prevent the agglomeration of nanoparticles are continuing (Dung et al. 2009). Li et al. (2008) synthesized nanoparticles by covalent binding of chitosan on the Fe_3O_4 nanoparticles through glutaraldehyde cross-linking. However, the agglomeration of the CS MNPs could not be prevented (Li et al. 2008).

Cell proliferation assay results proved that the synthesized nanoparticles (MNPs and CS MNPs) are

not cytotoxic on cancer cell lines (SiHa and HeLa). They may be suitable as magnetic nanocarriers in biomedical applications such as targeted drug delivery, magnetic resonance imaging (MRI), and magnetic hyperthermia.

There are important applications for small sized nanoparticles in the literature. Kim et al. (2005) have synthesized superparamagnetic magnetite by a sonochemical method. These particles were used as MRI agents by combining them with chitosan. These spherical particles were about 15 nm in diameter (Laurent et al. 2010). Kavaz et al. (2010) synthesized chitosan-coated Fe_3O_4 nanoparticles in the size of around 150 nm and they loaded Concavalin-A for targetting of cancer cells and Bloemycin as an anticancer agent. The utilization of small sized superparamagnetic nanoparticles for targeted drug delivery applications have been reported in the literature (Neuberger et al. 2005). The synthesized nanoparticles in this study have potential applications for such purposes.

Acknowledgments The support of Assist. Prof. Dr Bora Mavis for FTIR is gratefully acknowledged, as well as financial support by TÜBİTAK-TBAG(1001)/109T949.

References

Agnihotri SA, Mallikarjuna NN, Aminabhavi TM (2004) Recent advances on chitosan-based micro- and nanoparticles in drug delivery. J Control Release 100(1):5–28

Allen TM, Cullis PR (2004) Drug delivery systems: entering the mainstream. Science 303(5665):1818–1822

Bhattarai SR, Kc RB, Kim SY, Sharma M, Khil MS, Hwang PH, Chung GH, Kim HY (2008) *N*-hexanoyl chitosan stabilized magnetic nanoparticles: implication for cellular labeling and magnetic resonance imaging. J Nanobiotechnol 6:1

Bhumkar DR, Pokharkar VB (2006) Studies on effect of pH on cross-linking of chitosan with sodium tripolyphosphate. AAPS PharmSci Tech 7(2):E138–E143

Calvo P, Remuñan-López C, Vila-Jato JL, Alonso MJ (1997) Chitosan and chitosan/ethylene oxide-propylene oxide block copolymer nanoparticles as novel carriers for proteins and vaccines. Pharm Res 14(10):1431–1436

Coates J (2000) Encyclopedia of analytical chemistry. In: Meyers RA (ed) Interpretation of infrared spectra, a practical approach. Wiley, Chichester, pp 10815–10837

Corot C, Robert P, Idee JM, Port M (2006) Recent advances in iron oxide nanocrystal technology for medical imaging. Adv Drug Deliv Rev 58:1471–1504

Daou TJ, Pourroy G, Bégin-Colin S, Grenèche JM, Ulhaq-Bouillet C, Legaré P, Bernhardt P, Leuvrey C, Rogez G (2006) Hydrothermal synthesis of monodisperse magnetite nanoparticles. Chem Mater 18:4399–4404

Das M, Mishra D, Maiti TK, Basak A, Pramanik P (2008) Biofunctionalization of magnetite nanoparticles using an aminophosphonic acid coupling agent: new, ultradispersed, iron-oxide folate nanoconjugates for cancer-specific targeting. Nanotechnology 19(41):415101

Denkbas EB, Kilicay E, Birlikseven C, Ozturk E (2002) Magnetic chitosan microspheres: preparation and characterization. React Funct Polym 50:225–232

Dung DTK, Hai1 TH, Phuc LH, Long BD, Vinh LK, Truc PN (2009) Preparation and characterization of magnetic nanoparticles with chitosan coating, APCTP–ASEAN Workshop on Advanced Materials Science and Nanotechnology (AMSN08) IOP Publishing Journal of Physics: Conference Series 187, 012036

Florence AT, Hillery AM, Hussain N, Jani PU (1995) Nanoparticles as carriers for oral peptide absorption: studies on particle uptake and fate. J Control Release 36:39–46

Gupta AK, Wells S (2004) Surface-modified superparamagnetic nanoparticles for drug delivery: preparation, characterization, and cytotoxicity studies. IEEE Trans Nano Biosci 3:66–73

Hritcu D, Popa MI, Popa N, Badescu V, Balan V (2009) Preparation and characterization of magnetic chitosan nanospheres. Turk J Chem 33:785–796

Hu M, Li Y, Decker EA, Xiao H, McClements DJ (2010) Influence of tripolyphosphate cross-linking on the physical stability and lipase digestibility of chitosan-coated lipid droplets. J Agric Food Chem 58:1283–1289

Kavaz D, Odabas S, Guven E, Demirbilek M, Denkbas EB (2010) Bleomycin loaded magnetic chitosan nanoparticles as multifunctional nanocarriers. J Bioact Comp Poly 25:305–318

Kim EH, Lee HS, Kwak BK, Kim BK (2005) Synthesis of ferrofluid with magnetic nanoparticles by sonochemical method for MRI contrast agent. J Magn Magn Mater 289:328–330

Laurent S, Forge D, Port M, Roch A, Robic C, Elst LV, Muller RN (2010) Magnetic iron oxide nanoparticles: synthesis, stabilization, vectorization, physicochemical characterizations, and biological applications. Chem Rev 108:2064–2110

Lefevre ME, Vanderhoff JW, Laissue JA, Joel DD (1978) Accumulation of 2-mm latex particles in mouse Peyer's patches during chronic latex feeding. Cell Mol Life Sci 34:120–122

Li MC, Liu C, Xin M, Zhao H, Wang M, Feng Z, Sun X (2005) Preparation and characterization of acylated chitosan. Chem Res Chinese U 21(1):114–116

Li G, Jiang Y, Huang K, Ding P, Chen J (2008) Preparation and properties of magnetic Fe_3O_4–chitosan nanoparticles. J Alloy Compd 466:451–456

Liu R, Zhao Y, Huang R, Zhao Y, Zhou H (2010) Shape evolution and tunable properties of monodisperse magnetite crystals synthesized by a facile surfactant-free hydrothermal method. Eur J Inorg Chem 2010(28):4499–4505

Lu G, Kong L, Sheng B, Wang G, Gong Y, Zhang X (2007) Degradation of covalently cross-linked carboxymethyl chitosan and its potential application for peripheral nerve regeneration. Eur Polym J 43:3807–3818

Lubbe AS, Bergemann C, Riess H, Schriever F, Reichardt P, Possinger K et al (1996) Clinical experiences with

magnetic drug targeting: a phase I study with 4′-epidoxorubicin in 14 patients with advanced solid tumors. Cancer Res 56(20):4686–4693

Ma W, Ya F, Han M, Wang R (2007) Characteristics of equilibrium, kinetics studies for adsorption of fluoride on magnetic-chitosan particle. J Hazard Mater 143:296–302

Maaz K, Mumtaz A, Hasanain SK, Ceylan A (2007) Synthesis and magnetic properties of cobalt ferrite ($CoFe_2O_4$) nanoparticles prepared by wet chemical route. J Magn Magn Mater 308(2):289–295

Massart R, Cabuil V (1987) Synthèse en milieu alcalin de magnétite colloïdale: contrôle du rendement et de la taille des particules. J Chim Phys 84:961–973

Mornet S, Vasseur S, Grasset F, Duguet E (2004) Magnetic nanoparticle design for medical diagnosis and therapy. J Mater Chem 14:2161–2175

Neuberger T, Schopf B, Hofmann H, Hofmann M, Vonrechenberg B (2005) Superparamagnetic nanoparticles for biomedical applications: possibilities and limitations of a new drug delivery system. J Magn Magn Mater 293(1):483–496

Paama L, Pitkänen I, Halttunen H, Perämäki P (2003) Infrared evolved gas analysis during thermal investigation of lanthanum, europium and samarium carbonates. Thermochim Acta 403:197–206

Park JH, Saravanakumar G, Kim K, Kwon IC (2010) Targeted delivery of low molecular drugs using chitosan and its derivatives. Adv Drug Deliv Rev 62:28–41

Pison U, Welte T, Giersig M, Groneberg DA (2006) Nanomedicine for respiratory diseases. Eur J Pharmacol 533(1–3):341–350

Prabaharan M, Mano JF (2005) Chitosan-based particles as controlled drug delivery systems. Drug Deliv 12(1):41–57

Sanders E, Ashworth CT (1961) A study of particulate intestinal absorption and hepatocellular uptake. Exp Cell Res 22:114–137

Singh S, Pandey VK, Tewari RP, Agarwal V (2011) Nanoparticle based drug delivery system: advantages and applications. Ind J Sci Tech 4(3):167–169

Teng X, Black D, Watkins NJ, Gao Y, Yang H (2003) Platinum–maghemite core–shell nanoparticles using a sequential synthesis. Nano Lett 3(2):261–264

Tiaboonchai W, Limpeanchob N (2007) Formulation and characterization of amphotericin B-chitosan-dextran sulfate nanoparticles. Int J Pharm 329:142–149

Veiseh O, Gunn JW, Zhang M (2010) Design and fabrication of magnetic nanoparticles for targeted drug delivery and imaging. Adv Drug Deliv Rev 62:284–304

Wan Y, Creber KAM, Peppley B, Bui VT (2003) Synthesis, characterization and ionic conductive properties of phosphorylated chitosan membranes. Macromol Chem Physiol 204:850–858

Wang Y, Li B, Zhou Y, Jia D (2009) In situ mineralization of magnetite nanoparticles in chitosan hydrogel. Nanoscale Res Lett 4(9):1041–1046

Weinstein JS, Varallyay CG, Dosa E, Gahramanov S, Hamilton B, Rooney WD, Muldoon LL, Neuwelt EA (2010) Superparamagnetic iron oxide nanoparticles: diagnostic magnetic resonance imaging and potential therapeutic applications in neurooncology and central nervous system inflammatory pathologies, a review. J Cereb Blood Flow Metab 30:15–35

Weissleder R, Cheng H-C, Bogdanova A, Bogdanov A Jr (1997) Magnetically labeled cells can be detected by MR imaging. J Magn Reson Imaging 7:258–263

Wu Y, Wang Y, Luo G, Dai Y (2009) In situ preparation of magnetic Fe_3O_4–chitosan nanoparticles for lipase immobilization by cross-linking and oxidation in aqueous solution. Bioresour Technol 100(14):3459–3464

Xu H, Tong N, Cui L, Lu Y, Gu H (2007) Preparation of hydrophilic magnetic nanospheres with high saturation magnetization. J Magn Magn Mater 311:125–130

Ye XR, Daraio C, Wang C, Talbot JB, Jin S (2006) Room temperature solvent-free synthesis of monodisperse magnetite nanocrystals. J Nanosci Nanotechnol 6:852–856

Yezhelyev MV, Gao X, Xing Y, Al-Hajj A, Nie S, O'Regan RM (2006) Emerging use of nanoparticles in diagnosis and treatment of breast cancer. Lancet Oncol 7(8):657–667

Yuwei C, Jianlong W (2011) Preparation and characterization of magnetic chitosan nanoparticles and its application for Cu(II) removal. Chem Eng J 168:286–292

Zhang L, Zhu X, Sun H, Chi G, Xu J, Sun Y (2010a) Control synthesis of magnetic Fe_3O_4–chitosan nanoparticles under UV irradiation in aqueous system. Curr Appl Phys 10:828–833

Zhang XL, Niu HY, Zhang SX, Cai YQ (2010b) Preparation of a chitosan-coated C18-functionalized magnetite nanoparticle sorbent for extraction of phthalate ester compounds from environmental water samples. Anal Bioanal Chem 397:791–798